Available online at www.sciencedirect.com

ScienceDirect

Proceedings of the Combustion Institute 000 (2020) 1–8

Proceedings of the Combustion Institute

www.elsevier.com/locate/proci

Plasma-assisted ignition of methane/air and ethylene/air mixtures: Efficiency at low and high pressures

Nicholas Deak [a,*], Aurélie Bellemans [a,b], Fabrizio Bisetti [a]

[a] *Department of Aerospace Engineering and Engineering Mechanics, University of Texas at Austin, Austin, TX 78712, USA*

[b] *Département d'Aéro-Thermo-Mécanique, Ecole Polytechnique de Bruxelles, Université Libre de Bruxelles, Ixelles 1050, Belgium*

Received 7 November 2019; accepted 28 June 2020
Available online xxx

Abstract

The ignition of methane/air and ethylene/air mixtures by nanosecond pulsed discharges (NSPD) is investigated numerically using a zero-dimensional isochoric adiabatic reactor. A combustion kinetics model is coupled with a non-equilibrium plasma mechanism, which features vibrational and electronic excitation, dissociation, and ionization of neutral particles (O_2 and N_2) via electron impact. A time to ignition metric τ is defined, and ignition simulations encompassing a wide range of pressures (0.5–30 atm) and pulsing conditions for each fuel are executed. For each fuel, it is found that τ depends primarily on initial pressure and energy deposition rate, and scaling laws are derived. In order to quantify the benefit gained from plasma-assisted ignition (PAI), τ is compared with a thermal ignition time. It is found that for both fuels, PAI leads to a faster ignition at low pressures, while at higher pressures ($p_0 \geq 5$ atm), methane/air ignition becomes inefficient (meaning a longer ignition time for the same input energy compared to thermal ignition). Ethylene/air PAI shows only a modest deterioration. The drop in performance with pressure is found to be due to the mean electron energy achieved during the pulse, which shows an inverse relationship with pressure, leading to fewer excited species and combustion radicals. The poor performance of methane/air mixture ignition at high pressure is explained by an analysis of the reaction pathways. At high pressures ($p_0 \sim 30$ atm), H is consumed mostly to form hydroperoxyl (HO_2), leading to a bottleneck in the formation of formyl (HCO) from formaldehyde (CH_2O). Instead, for ethylene/air ignition, at both low and high pressures there exist several bypass pathways that facilitate the formation of HCO and CO directly from various intermediates, explaining the more robust performance of PAI for ethylene at pressure.

Keywords: Plasma assisted combustion; Nanosecond repetitively pulsed discharge; Non-equilibrium plasma; Chemical kinetics

* Corresponding author.
E-mail address: ndeak@utexas.edu (N. Deak).

https://doi.org/10.1016/j.proci.2020.06.126
1540-7489

1. Introduction

The ability to ignite a reactive mixture reliably and stabilize turbulent flames is of critical importance in most combustion devices. Combustion in air-breathing high-speed vehicles and systems is characterized by low pressures ($\mathcal{O}(0.1-1\,\text{atm})$) and short residence times ($\mathcal{O}(1\,\text{ms})$), making ignition and flame anchoring challenging [1]. A second set of applications is ultra-lean combustion in internal combustion engines and gas turbines, which is characterized by elevated pressures $\mathcal{O}(10-100\,\text{atm})$ and lean premixed or statified mixtures of large hydrocarbons found in transportation fuels. In internal combustion engines in particular, ultra-lean and statified operation makes conventional ignition systems impractical and has encouraged the development of alternative ignition approaches [2]. For ultra-lean gas turbine combustors, thermo-acoustic instabilities are a key challenge, which may be addressed with local energy deposition and active control of flame dynamics.

Non-equilibrium plasmas (NEP), which feature electron temperatures that exceed the background gas temperature, have emerged as a promising tool for ignition and energy deposition [3]. Unlike traditional ignition techniques, which rely mostly on gas heating, NEP provides enhancement through kinetics. This occurs through collisions between energetic electrons and abundant particles such as diatomic nitrogen and oxygen (O_2 and N_2), ultimately leading to the generation of radicals that promote ignition (namely O, H, and OH). Nanosecond pulsed discharges (NSPD) are particularly effective, as they feature high reduced electric fields ($\mathcal{O}(100-1000)\,\text{Td}$)), leading to highly energetic electrons ($\gg 1$ eV).

Understanding the dynamics of plasma-assisted ignition (PAI) over a wide range of conditions is an area of active research. Various 2D and 3D numerical studies have been conducted [4,5] to explore aspects of plasma-assisted combustion (PAC), but have been limited to H_2/O_2 and H_2/air mixtures or employed semi-empirical models for plasma discharges. Experimental studies have been conducted for hydrogen (H_2) [6,7], methane (CH_4) [8,9], ethylene (C_2H_4) [10–12], and higher hydrocarbon [13] fuel mixtures. The focus has largely been on developing accurate kinetic mechanisms and most of these studies have been conducted at low pressures ($p \leq 1$ atm), with a focus on low temperature combustion pathways. Fundamental questions remain, regarding the ideal pulsing strategy, and how performance changes under different pressures and equivalence ratios.

The goal of this paper is to explore how fuel type, pressure, and pulse parameters impact ignition behavior. This is accomplished with a two-temperature zero-dimensional reactor model, which is coupled to a state-of-the-art kinetics mechanism, which includes non-thermal plasma and combustion kinetics.

2. Physical models and numerical methods

The ignition of methane/air and ethylene/air mixtures via NSPD is simulated in a zero-dimensional isochoric adiabatic reactor with a mechanism featuring non-thermal plasma and combustion kinetics. A two-temperature model describes the non-thermal plasma generated during each pulse, as the strong electric field allows electrons to attain temperatures that are much higher than those of all other particles.

On the short time scale of a single nanosecond discharge, the transport of ions and other neutral particles is negligible and spatial inhomogeneities in the concentrations of particles other than electrons are due to plasma kinetics rather than particle transport. Thus, while a zero-dimensional reactor model does not include transport effects, it describes energy exchanges due to plasma processes at the head of streamers and in the quasi-neutral streamer body. Zero-dimensional plasma kinetics models are a well established approach in the study of chemical plasmas [6].

The mathematical model consists of a set of ordinary differential equations (ODEs) that describe the evolution of the thermodynamic state of an ensemble of M species. The number density of each particle class is n_i, the internal energy density of the electrons is u_e, and u is the internal energy density of the ensemble of all other particles. The system of $M+2$ ODEs reads

$$\frac{dn_i}{dt} = \omega_i \quad i = 1, \ldots, M, \tag{1}$$

$$\frac{du_e}{dt} = Q_e \qquad \frac{du}{dt} = Q. \tag{2}$$

In the equations above, ω_i is the net rate of formation of particle i and Q_e and Q are the rate of energy gain for the electrons and all other particles. The electron energy source term reads

$$Q_e = 3k_B\left(\sum_{i=1,\, i\neq e}^{M} \nu_i^{el}\frac{m_e}{m_i}\right) n_e(T_e - T) - \sum_{j=1}^{R} \delta\varepsilon_j \omega_e^j + Q_E(t). \tag{3}$$

The first and second terms in Eq. (3) represent energy transfers from electrons to other particles via elastic and inelastic collisions, respectively. m_i and m_e are the masses of species i and electron mass, ν_i^{el} is the elastic collision frequency between species i and the electron, T_e and T are the temperature of the electron and that of all other particles. $\delta\varepsilon_j$ is the energy lost by the electron in inelastic collision

Please cite this article as: N. Deak, A. Bellemans and F. Bisetti, Plasma-assisted ignition of methane/air and ethylene/air mixtures: Efficiency at low and high pressures, Proceedings of the Combustion Institute, https://doi.org/10.1016/j.proci.2020.06.126

j occurring at a rate ω_e^j. The third term in Eq. (3), $Q_E(t)$, represents the energy acquired by electrons from the electric field during each pulse. The internal energy source term for the ensemble of particles other than the electrons is $Q = -Q_e + Q_E(t)$.

The discharge consists of a sequence of pulses at frequency f. The energy density per unit volume deposited by each pulse is E. The pulse power has a Gaussian profile with full-width-half-max FWHM. Pulses are centered at discrete times $t_k = t_1 + (k-1)/f$ with $k = 2, \ldots, K$. Thus, t_1 indicates the timing of peak power during the first pulse.

Thermodynamic properties and rate coefficients for all plasma processes and conventional combustion chemistry reactions are stored in CHEMKIN format and evaluated using the two-temperature extension of the CHEMKIN library [14]. More details about the kinetics model are provided below in Section 2.1. Time integration of the system of ODEs is performed efficiently with a variable time step and variable order Backward Differentiation Formula (BDF) implicit method as implemented in the CVODE solver [15].

2.1. Kinetics mechanism

The kinetics mechanism of Eckert et al. [16] for PAC applications is used in this study. The mechanism includes the electron, 2 ions (O_2^+ and N_2^+), 160 neutral species, and 1167 reactions and features various classes of electron/particle processes as well as conventional combustion chemistry. The combustion model describes the oxidation of H_2, CH_4, C_2H_4, and C_3H_8 and has been validated for fuel lean and fuel rich conditions at low and high temperatures and pressures up to 40 atm [17].

The set of plasma kinetics includes electron impact processes, whereby energetic electrons collide with ground state species (O_2, N_2, O, H_2, CH_4, C_2H_2, C_2H_4, C_3H_8), resulting in particle excitation, dissociation, and ionization. Vibrational excitation is included for N_2, for which the first 8 vibrational levels are considered, along with electronically excited levels for O_2, N_2, and O, and corresponding de-excitation reactions. Reactions describing electron interactions with radicals and combustion products have been omitted in order to reduce the mechanism complexity at this stage.

The rate coefficients of collisions involving electrons and heavy species depend on the electron temperature and are not well-described by the Arrhenius form, necessitating special functional fits. The rate coefficients for all processes involving high-energy electrons in the mechanism from Ref. [16] were recomputed using the most recent cross section data from the LxCat database [18] and the Boltzmann kinetics solver BOLSIG+ [19], and parametrized as a function of T_e, using the JANEV functional forms available in CHEMKIN. The mechanism along with updated reactions is available as supplemental material.

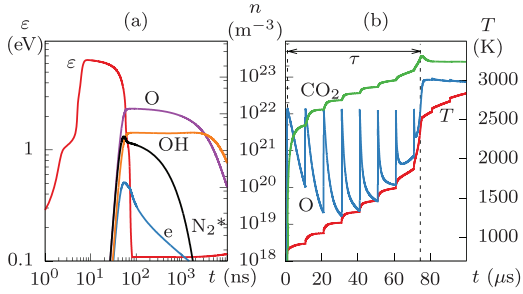

Fig. 1. Time evolution of the mean electron energy ε, number density of select species and gas temperature during ignition of a 0.5 atm stoichiometric methane/air mixture for (a) a single pulse and (b) multiple pulses ($E = 31.9$ mJ cm^{-3}, FWHM = 15 ns, and $f = 100$ kHz).

As described in [20], data from a series of low pressure ($\lesssim 1$ atm) experiments have been used to validate the mechanism extensively. The cross sections used by BOLSIG+ to model electron/neutral collisions are not measured or obtained theoretically at elevated pressures ($\gg 1$ atm), however it is generally understood that pressure effects are less important for two-body electron/molecule interactions. Quenching of vibrationally and electronically excited nitrogen and oxygen may be impacted by elevated pressure, but the data in the literature are scarce.

3. Results

3.1. Preliminaries and overview

PAI of fuel/air mixtures via NSPD is simulated with a two-temperature isochoric and adiabatic reactor. For all cases, the initial temperature T_0 is 800 K, which is representative of applications in power generation and hypersonics alike. The study considers methane and ethylene fuels, various stoichiometries, and initial pressures p_0 from 0.5 to 30 atm. While it is known that at elevated pressures, plasma streamers exhibit modified behavior, as they become filamentary in nature and the deposition of energy becomes less homogenous [21], these effects are are ignored in the present 0D study.

The discharge parameters are varied across a range of values that guarantee ignition within 100 μs. Discharge frequencies between 5 and 500 kHz, FWHM between 15 and 60 ns, and single pulse energy densities between 15 and 15,000 J / cm^3 are explored. A wide range of energy densities is explored due to the wide range of pressures. The reactor is initialized with pressure $p = p_0$, temperature $T = T_e = T_0$, and a mixture of fuel and air with equivalence ratio Φ.

Figure 1 presents an overview of the temporal evolution of the reactive mixture during a NSPD

Please cite this article as: N. Deak, A. Bellemans and F. Bisetti, Plasma-assisted ignition of methane/air and ethylene/air mixtures: Efficiency at low and high pressures, Proceedings of the Combustion Institute, https://doi.org/10.1016/j.proci.2020.06.126

and is characteristic of all ignition events considered in this study. The values of energy density per pulse employed in the study are comparable to those in experimental studies on PAI. Lefkowitz et al. [22] report using 0.8–3.2 mJ per pulse in a discharge channel volume of ~ 17 mm^{3}to ignite a mixture of methane and air at 1 atm and 850 K.

During each discharge, the electrons reach peak mean energies $\varepsilon \approx 6.5$ eV (before which an inflection corresponding to rapid vibrational excitation of N_2 is observed), followed by rapid cooling. Energetic electrons form excited state particles, mostly of O_2 and N_2 and the quenching reactions that follow excitation (e.g. $N_2^* + O_2 \rightarrow N_2 + 2O$) result in the formation of radicals as the excited particles thermalize. This process is known as *ultra-fast heating* [23], marked by a modest increase in T.

Across multiple pulses, radicals and transient species exhibit sawtooth profiles shown by the O radical. As reactants are consumed, the peak concentrations of combustion radicals during each pulse decrease, though this trend is not visible in the log scale in Fig. 1. After a number of pulses, the concentration of carbon dioxide increases abruptly, signaling that conventional exothermic reactions undergo a rapid acceleration consistent with an *ignition event*. Thus, the instant in time when the rate of change of the number density of CO_2 peaks is taken to represent the time of ignition t^*. Then, the *time to ignition* (TTI) is defined as $\tau = t^* - t_1$, where t_1 is the timing of the peak discharge power during the first pulse. Thus, τ represents the interval between the first pulse and ignition. Following ignition, the gas temperature continues increasing due to the relaxation of the remaining excited species, eventually reaching a thermochemical equilibrium.

Achieving fast and reliable ignition requires understanding the factors that impact τ most. We found that fuel type, mean energy deposition rate $W = Ef$, and initial pressure p_0 account for most of the variation in the time to ignition across cases.

Fig. 2 shows τ for stoichiometric mixtures of methane/air and ethylene/air at 800 K and several combinations of $15 \le E \le 15,000$ J cm^{-3}, $5 \le f \le 500$ kHz, $15 \le \text{FWHM} \le 60$ ns, and $0.5 \le p_0 \le 30$ atm. The data are reported in compensated form $\tau/(p_0/p^*)^b$ versus W/W^*, where $p^* = 1$ atm and $W^* = 10$ kJ cm^{-3} s^{-1} are reference quantities. Fits of the form $\tau = C(W/W^*)^a(p_0/p^*)^b$ are shown alongside the data from simulations and the parameters are provided in the caption for methane and ethylene.

Several important conclusions can be drawn from Fig. 2. First, τ depends on the energy deposition rate $W = Ef$ and not on the energy density per pulse E and pulse frequency f, separately. In other words, less energetic and more frequent pulses are equivalent to more energetic and less frequent pulses. Second, τ decreases as the mean energy deposition rate W increases, so that faster

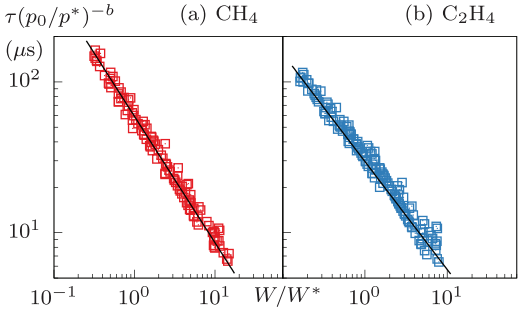

Fig. 2. Compensated time to ignition $\tau/(p_0/p^*)^b$ for (a) methane/air and (b) ethylene/air stoichiometric mixtures ($T_0 = 800$ K, $15 \le \text{FWHM} \le 60$ ns) as a function of the dimensionless mean energy deposition rate W/W^* alongside fits of the form $\tau = C(W/W^*)^a(p_0/p^*)^b$: $C = 59$ μs, $a = -0.84$, and $b = 0.87$ for methane and $C = 29.9$ μs, $a = -0.72$, and $b = 0.66$ for ethylene.

ignition is achieved by either increasing energy density E or frequency f. Third, the power law model is broadly consistent with the ignition behavior of the two reactive mixtures, so that $\tau \sim p_0^b$ at constant mean energy deposition rate and $\tau \sim W^a$ at constant pressure. The agreement is rather convincing, especially because the ranges of values spanned by τ, W and p_0 are broad, encompassing values relevant to applications.

Finally, the response of τ to changes in p_0 and W, pressure and power, are distinctly different for methane and ethylene. According to the model, $W \sim p_0^{-b/a}$ for constant τ, so that $-b/a = 1.04$ for methane and $-b/a = 0.92$ for ethylene, pointing to the fact that the energy per unit mass of the mixture required to keep τ constant increases as pressure increases for methane/air, while it decreases for ethylene/air mixtures. This highlights an important sensitivity of the kinetics of PAI to pressure and fuel type.

While not explored in this paper, τ displays secondary dependencies on other pulsing parameters, namely the pulse FWHM and frequency f. Specifically, it is found that for a given energy deposition rate, shorter and stronger pulses at a lower frequency lead to the fastest ignitions. These secondary effects are explored in [24].

3.2. Pressure effects on plasma and combustion kinetics

In order to separate the contributions of plasma kinetics and combustion chemistry to the dependence of τ on pressure, we conducted additional simulations with direct heating of the gas. In these auxiliary simulations, the power Q_E is delivered directly to the gas, defined here as the collection of all particles other than electrons. This approach results in thermal heating of the mixture on the same time scales of the discharge pulses without the

Please cite this article as: N. Deak, A. Bellemans and F. Bisetti, Plasma-assisted ignition of methane/air and ethylene/air mixtures: Efficiency at low and high pressures, Proceedings of the Combustion Institute, https://doi.org/10.1016/j.proci.2020.06.126

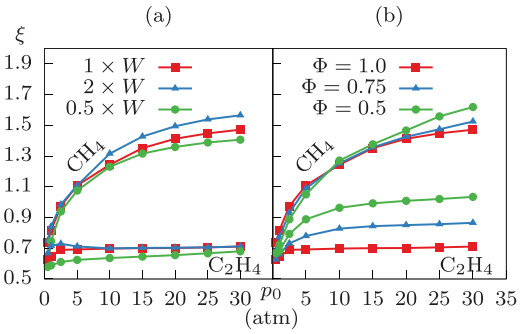

Fig. 3. Ratio of time to ignition $\xi = \tau/\tau_T$ for methane/air and ethylene/air as a function of p, keeping the energy per unit mass constant. The effect of (a) energy and (b) equivalence ratio are shown.

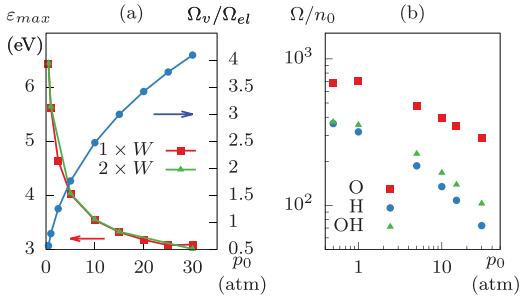

Fig. 4. (a) Peak value of the mean electron energy $\varepsilon_{\max}$ during the first discharge pulse for two sets of power deposition rates, and ratio of vibrational excitation losses (Ω_v), to electronic excitation losses (Ω_{el}) averaged over the first pulse, as a function of pressure. (b) Average radical production (kmol/m^3-s) for the dataset described in Section 3.2, normalized by initial number density n_0 for CH_4.

generation of high-energy electrons responsible for the production of radicals.

The time to ignition with direct gas heating is indicated with τ_T and the ratio $\xi = \tau/\tau_T$ is defined and shown in Fig. 3 as a function of pressure for the two fuels, mixtures of varying stoichiometry, and several mean energy deposition rates. The data are obtained as follows. Starting from $p_0 = 0.5$ atm and $W = 34$ kJ cm^{-3} s^{-1}, the pressure is varied and W is adjusted in order to keep the mean energy deposition rate per unit mass constant. The FWHM is held constant and equal to 15 ns and the frequency is $f = 100$ kHz for all cases. The same simulations are repeated for $\Phi = 1.0, 0.75, 0.5$, and for higher and lower values of W in order to explore the dependence of ξ on Φ and W.

The following trends are apparent in Fig. 3. First, $\xi \leq 1.0$ for nearly all ethylene/air mixtures and all cases considered, indicating that PAI of ethylene is energetically more *efficient* than ignition via direct gas heating (meaning the same power deposition leads to a faster ignition). Interestingly, the same remains true even as pressure increases, which suppresses radical production as discussed later. Nonetheless, ξ does display a minor increase with increasing pressure. Second, $\xi < 1$ at low pressures ($p_0 < 3$ atm) for methane/air mixtures, while ξ becomes greater than unity and continues to grow as pressure rises. This trend points to a loss of efficiency of PAI of methane for higher pressures. Third, the two conclusions hold true qualitatively even as the equivalence ratio and the mean energy deposition rate change. Fourth, a dependence of ξ on ϕ for C_2H_4 ignition is observed, as decreasing Φ leads to less C_2H_4 oxidation, lower amounts of heat release, and thus less efficient ignition.

To conclude, PAI loses its advantages in terms of shorter τ as pressure increases, but the value and rate of increase of the ratio τ/τ_T differ significantly for methane/air and ethylene/air mixtures. The remainder of the paper is devoted to explaining this behavior.

3.3. Radical production

One primary mechanism leading to loss of efficiency for PAI as pressure increases is related to the dependence of the peak mean electron energy $\varepsilon_{\max}$ on pressure p_0. As shown in Fig. 4a, the peak mean electron energy drops rapidly as pressure increases, and this behavior is not sensitive to W, and fuel type (not shown).

The decrease in ε_{max} with pressure has important implications for the generation of excited species and radical production. The electron energy distribution function and the associated mean electron energy control electron/particle interactions. This is due to the fact that inelastic collisions have specific energy thresholds. Vibrational excitation of N_2 requires an electron energy in the range of 0.1–3 eV, while electronic excitation of N_2, dissociation, and ionization require higher energies, in the range of 6–16 eV.

Thus, the lower the pressure, the higher the mean electron energy and the greater the rates of production of electronically excited N_2, which is efficient at creating O radicals through collision with O_2. Conversely, as pressure increases, the discharge energy contributes mostly to the vibrational excitation of N_2, which does not lead to the production of radicals. This also explains the energy budgets in less efficient ignition cases (for a given input energy).

The dependence of the so-called *energy branching* of the plasma discharge on pressure is well known and shown in Fig. 4a, which depicts the ratio of electronic and vibrational electron energy losses (Ω_{el}/Ω_v), averaged over 10 μs (one pulse).

The impact this has on the generation of radicals is demonstrated in Fig. 4b, which shows the pulse-averaged rate of production of combustion radicals as a function of pressure. The rate of

Please cite this article as: N. Deak, A. Bellemans and F. Bisetti, Plasma-assisted ignition of methane/air and ethylene/air mixtures: Efficiency at low and high pressures, Proceedings of the Combustion Institute, https://doi.org/10.1016/j.proci.2020.06.126

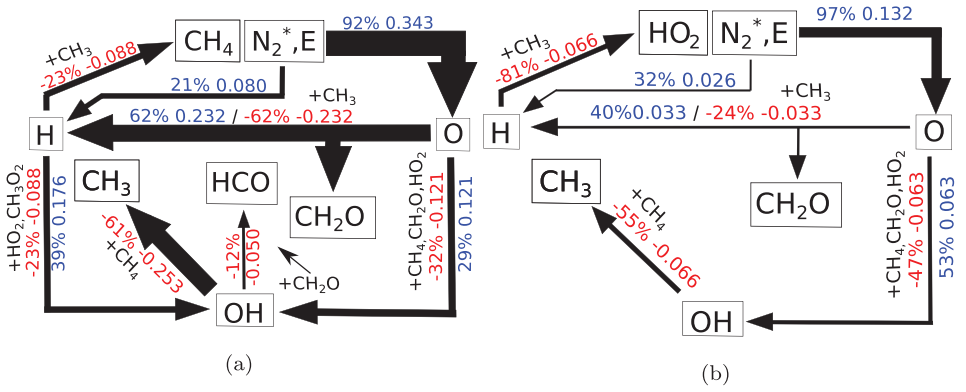

Fig. 5. Pathway analysis for O, H and OH during CH_4 ignition, averaged over the first two pulses for (a) 0.5 atm and (b) 30 atm, with the same pulsing conditions in Section 3.2. Percentages of production (blue) and consumption (red) are shown, along with average rates normalized by the initial number density n_0. Arrow thickness is proportional to the average rate.

production is normalized by the initial number density n_0 in order to compensate for the increase in mixture density brought by pressure. It is apparent that the normalized rate of formation of all three radicals decreases as pressure increases. A similar decrease in the rates of formation of radicals in ethylene/air mixtures is found (not shown).

A comprehensive analysis of the kinetics processes responsible for the loss of efficiency of PAI in methane/air mixtures with pressure and the resilience of the same PAI in ethylene/air is presented next by considering detailed pathways for low and high pressure ignition cases. The low pressure case features $p_0 = 0.5$ atm and $W = 34$ kJ cm^{-3} s^{-1}, while the high pressure case features $p_0 = 30$ atm and $W = 2.04$ MJ cm^{-3} s^{-1}, so that the mean energy deposition rate is scaled in order to keep the energy per unit mass constant.

In Fig. 5, nodes indicate species and arrows indicate reactions. For the sake of clarity, only the major pathways are shown. For each plot, the thickness of the arrows is proportional to the normalized rate of progress of the specific reaction averaged over 20 μs (two pulses). The rates are normalized by n_0 to account for variations brought by density and pressure and facilitate comparisons between the low and high pressure cases. Percentages next to the rates are computed for each reaction relative to the total rate of formation (positive numbers) or total rate of destruction (negative numbers) for the radicals involved in each reaction.

We begin by considering the pathways involving O, H, and OH in Fig. 5a and b, respectively. While the data are shown for methane/air ignition similar results are obtained for ethylene/air on the account that the plasma reactions involved pertain to air mostly.

Plasma reactions are responsible for 92% to 96% of the rate of formation of O and for a more modest contribution to H (20–32% at low and high pressure), mainly through collisions of CH_4 with electrons and electronically excited N_2. We find that O radicals are crucial in the breakdown of methyl radicals through $CH_3 + O \rightarrow CH_2O + H$, which is also an important source of H. O promotes ignition via attacks on methane to form methyl ($CH_4 + O \rightarrow CH_3 + OH$) and on formaldehyde to produce formyl ($CH_2O + O \rightarrow HCO + OH$). At low pressure, H contributes to the formation of OH via the breakdown of hydroperoxyl ($HO_2 + H \rightarrow 2OH$). These sources of OH account for 2/3 of the overall production of OH, which is the radical most involved in the abstraction of hydrogen from CH_4.

At this point, it is important to recall that methane oxidation to carbon monoxide proceeds through a sequence of intermediates, $CH_4 \rightarrow CH_3 \rightarrow CH_2O \rightarrow HCO \rightarrow CO$, whereby the first three steps require radicals. First hydrogen abstraction from CH_4 to form the methyl radical CH_3 requires any one of O, H, or OH. Next, the formation of CH_2O is mostly due to $CH_3 + O \rightarrow CH_2O + H$. Most importantly, the key step $CH_2O + H \rightarrow HCO + H_2$ requires the H radical. The formyl radical then reacts with O_2 to form CO.

In the high-pressure case, H is consumed by the reaction $H + O_2 \rightarrow HO_2$ instead, which is a well known chain-termination step given that HO_2 is a rather stable species. Thus, regardless of the rates of formation of O and, subsequently, of all other radicals, the destruction of H to form HO_2 conspires to slow down the conversion of formaldehyde to formyl. At low pressure, this is the largest source of HCO, accounting for 41% of production. Instead, it becomes insignificant as pressure increases. Since this is the primary pathway for HCO production, this bottleneck also limits the production of CO and ultimately CO_2, severely mitigating the benefits of radicals produced via discharges. For every mole of methane converted to methyl, less than

Please cite this article as: N. Deak, A. Bellemans and F. Bisetti, Plasma-assisted ignition of methane/air and ethylene/air mixtures: Efficiency at low and high pressures, Proceedings of the Combustion Institute, https://doi.org/10.1016/j.proci.2020.06.126

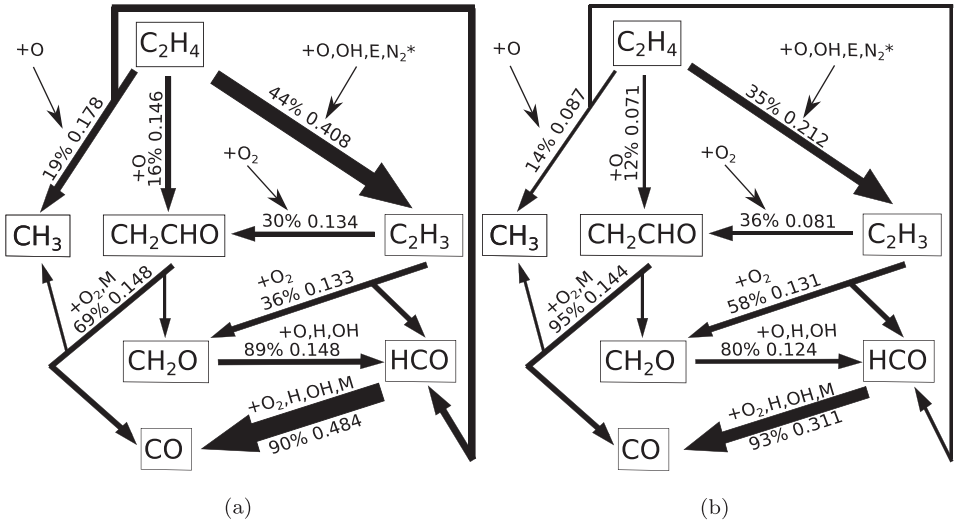

Fig. 6. Pathway analysis for C_2H_4 ignition, averaged over the first two pulses for (a) 0.5 atm and (b) 30 atm, with the same pulsing conditions in Section 3.2.

0.09 moles of CO are created at high pressure. In contrast, around 0.29 moles of CO are created for each mole of CH_3 at low pressure.

Although not shown, the pathways of radical formation and consumption are very similar for ethylene/air mixtures. In particular, the same pathways leading to the consumption of H to form HO_2 are active in ethylene/air mixtures at high pressure also, but they appear to be inconsequential to the efficiency of PAI. As shown in Fig. 3, the ignition of stoichiometric ethylene/air mixtures via plasma discharges and radical production is not hindered significantly at high pressure compared to direct gas heating. The motivation for this peculiar behavior lies in the more complex network of reactions that lead to the formation of HCO in ethylene/air mixtures compared to methane/air.

Figure 6 shows the pathways of ethylene oxidation at low pressure. Compared to methane, ethylene oxidation occurs through a more complex network of reactions, starting with the initial H-abstraction from ethylene, primarily through attacks by O and OH. This results in the formation of ethylenyl C_2H_3 ($C_2H_4 + O \rightarrow C_2H_3 + OH$ and $C_2H_4 + OH \rightarrow C_2H_3 + H_2O$), vinoxy CH_2CHO ($C_2H_4 + O \rightarrow CH_2CHO + H$), and methyl radicals ($C_2H_4 + O \rightarrow CH_3 + HCO$). In particular, the last of these reactions is significant, as it bypasses the bottleneck $CH_2O \rightarrow HCO$ and allows for the direct formation of HCO, which is then converted to CO.

Ethylenyl is attacked primarily by O_2 to form vinoxy CH_2CHO ($C_2H_3 + O_2 \rightarrow CH_2CHO + O$) and formaldehyde and HCO ($C_2H_3 + O_2 \rightarrow CH_2O + HCO$). The former reaction is an important source of additional O radicals, while the latter reaction is a second bypass pathway leading to the formation of HCO. Two additional bypass reaction pathways leading to HCO involve the breakdown of CH_2CHO by O_2, ultimately forming CO and CH_2O through a complex set of reactions, and directly via $CH_2CHO + (M) \rightarrow CH_2O + CO$.

Because the three bypass pathways described above remain active at high pressure, ethylene ignition is largely unaffected by the loss of H radical to form HO_2. In particular, at 30 atm, for every mole of ethylene that undergoes hydrogen abstraction, about 0.99 moles of CO are created compared to 0.86 moles at 0.5 atm. This finding is consistent with faster ethylene/air ignitions for ethylene at high pressure (when keeping the energy density per unit mass of the mixture constant) and in contrast with methane. The bypass of the step $CH_2O + H \rightarrow HCO + H_2$ is key to explaining both the shorter time to ignition for ethylene/air compared to methane/air, as well as the persistent efficiency of PAI of ethylene at elevated pressures.

4. Conclusions

Ignition of methane/air and ethylene/air mixtures was simulated in a zero-dimensional reactor, with a kinetic model that couples non-thermal plasma and combustion kinetics. A wide range of pressures and pulsing conditions are explored and it is found that the time to ignition τ depends strongly on fuel type, initial pressure, and energy deposition rate. τ is compared with the thermal ignition time τ_T, and it is observed that plasma-assisted ignition (PAI) is more efficient at low pressures for both fuels. PAI becomes relatively less

Please cite this article as: N. Deak, A. Bellemans and F. Bisetti, Plasma-assisted ignition of methane/air and ethylene/air mixtures: Efficiency at low and high pressures, Proceedings of the Combustion Institute, https://doi.org/10.1016/j.proci.2020.06.126

efficient with increasing pressure, with this trend being more apparent for methane/air mixtures. The decrease in performance with pressure is tied to the peak mean electron energy during the pulse, which decreases with increasing pressure, leading to fewer excited species, and thus fewer combustion radicals (on a normalized basis). The poor performance of PAI for methane/air mixtures at high pressure (30 atm) is due to an inability to generate HCO from formaldehyde efficiently, caused by a lack of available H, which is converted to HO_2 by O_2 at high pressures. On the other hand, ethylene/air mixtures are more resilient to increasing pressure due to several bypass reaction pathways, which allow for the generation of HCO and CO from ethylene, ethylenyl, and vinoxy, thus circumventing the $CH_2O \rightarrow$ HCO bottleneck.

Declaration of Competing Interest

None.

Acknowledgments

Nicholas Deak and Fabrizio Bisetti are supported in part by NSF grant 1903775. Aurélie Bellemans is supported by a fellowship through the Belgian American Educational Foundation and the F.R.S - FNRS (Belgian Fund for Research).

Supplementary material

Supplementary material associated with this article can be found, in the online version, at doi:10.1016/j.proci.2020.06.126.

References

[1] S.B. Leonov, D.A. Yarantsev, *Plasma Sources Sci. Technol.* 16 (1) (2006) 132.
[2] B. Wolk, A. DeFilippo, J.-Y. Chen, R. Dibble, A. Nishiyama, Y. Ikeda, *Combust. Flame* 160 (7) (2013) 1225–1234.
[3] Y. Ju, W. Sun, *Prog. Energy Combust. Sci.* 48 (2015) 21–83.
[4] F. Tholin, D.A. Lacoste, A. Bourdon, *Combust. Flame* 161 (5) (2014) 1235–1246.
[5] L.L. Massa, J.B. Freund, in: 54th AIAA Aerospace Sciences Meeting, 2016, p. 2154.
[6] K. Togai, N. Tsolas, R.A. Yetter, *Combust. Flame* 164 (2016) 239–249.
[7] C. Winters, Y.-C. Hung, E. Jans, Z. Eckert, K. Frederickson, I.V. Adamovich, N. Popov, *J. Phys. D* 50 (50) (2017) 505203.
[8] C. Winters, Z. Eckert, Z. Yin, K. Frederickson, I. Adamovich, *J. Phys. D* 51 (1) (2017) 015202.
[9] Z. Eckert, N. Tsolas, K. Togai, A. Chernukho, R.A. Yetter, I.V. Adamovich, *J. Phys. D Appl. Phys.* 51 (37) (2018) 374002.
[10] S. Yang, X. Gao, V. Yang, W. Sun, S. Nagaraja, J.K. Lefkowitz, Y. Ju, *J. Propul. Power* (2016) 1240–1252.
[11] J.K. Lefkowitz, M. Uddi, B.C. Windom, G. Lou, Y. Ju, *Proc. Combust. Inst.* 35 (3) (2015) 3505–3512.
[12] N. Tsolas, R.A. Yetter, I.V. Adamovich, *Combust. Flame* 176 (2017) 462–478.
[13] A. Rousso, X. Mao, Q. Chen, Y. Ju, *Proc. Combust. Inst.* 37 (4) (2019) 5595–5603.
[14] R.J. Kee, F.M. Rupley, J.A. Miller, Chemkin-II: aFortran Chemical Kinetics Package for the Analysis of Gas-phase Chemical Kinetics, *Technical Report*, Sandia National Labs., Livermore, CA (USA), 1989.
[15] A.C. Hindmarsh, P.N. Brown, K.E. Grant, S.L. Lee, R. Serban, D.E. Shumaker, C.S. Woodward, *ACM Trans. Math. Softw.* 31 (3) (2005) 363–396.
[16] Z.S. Eckert, *Energy Transfer in Non-Equilibrium Reacting Gas Flows: Applications in Plasma Assisted Combustion and Chemical Gas Lasers* Ph.D. thesis, The Ohio State University, 2018.
[17] A.A. Konnov, *Combust. Flame* 156 (11) (2009) 2093–2105.
[18] S. Pancheshnyi, S. Biagi, M. Bordage, G. Hagelaar, W. Morgan, A. Phelps, L. Pitchford, *Chem. Phys.* 398 (2012) 148–153.
[19] G. Hagelaar, L. Pitchford, *Plasma Sources Sci. Technol.* 14 (4) (2005) 722.
[20] I.V. Adamovich, T. Li, W.R. Lempert, *Philos. Trans. R. Soc. A* 373 (2048) (2015) 20140336.
[21] S. Shcherbanev, C. Ding, S. Starikovskaia, N. Popov, *Plasma Sources Sci. Technol.* 28 (6) (2019) 065013.
[22] J.K. Lefkowitz, P. Guo, T. Ombrello, S.H. Won, C.A. Stevens, J.L. Hoke, F. Schauer, Y. Ju, *Combust. Flame* 162 (6) (2015) 2496–2507.
[23] I. Shkurenkov, I.V. Adamovich, *Plasma Sources Sci. Technol.* 25 (1) (2016) 015021.
[24] N. Deak, A. Bellemans, F. Bisetti, Ignition of methane and ethylene via nanosecond pulsed discharges, *AIAA 2020 SciTech Forum*, 2020.

Please cite this article as: N. Deak, A. Bellemans and F. Bisetti, Plasma-assisted ignition of methane/air and ethylene/air mixtures: Efficiency at low and high pressures, Proceedings of the Combustion Institute, https://doi.org/10.1016/j.proci.2020.06.126